

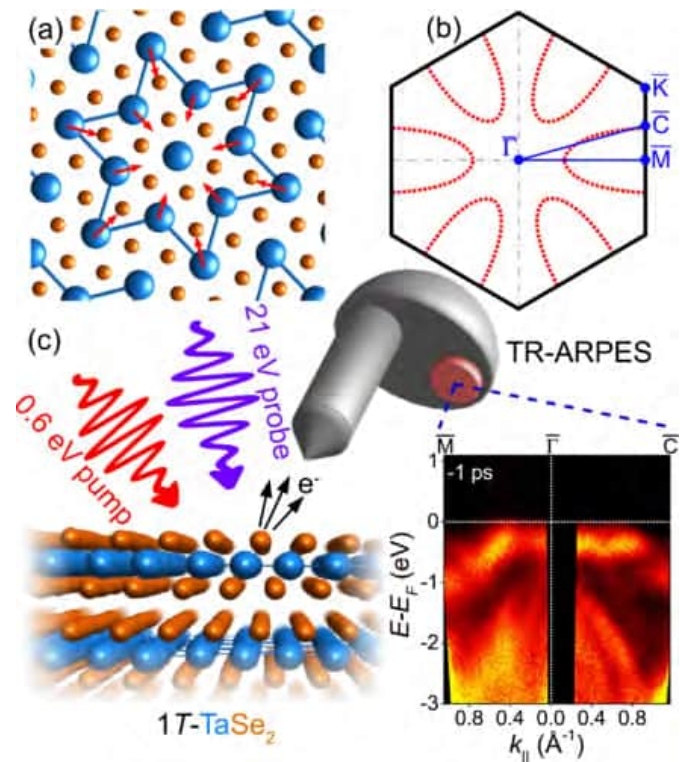
Imaging and Dynamics for Physical and Life Sciences

Exploring the Charge Density Wave Phase of 1T-TaSe₂: Mott or Charge-Transfer Gap?

The quest for finding quantum materials with unconventional electronic structures and on demand electrical switching has highlighted 2D tantalum-based dichalcogenides as systems with interesting metal to insulator transitions. 1T-TaSe₂ is widely believed to host a Mott metal-insulator transition in the charge density wave (CDW) phase according to the observation of a band gap that extends across all momentum space. At CLF-Artemis we combined time- and angle-resolved photoemission spectroscopy to gain new insights on the electronic structure and dynamics of this material. Our experiment probes the conduction band, previously ascribed to the upper Hubbard band, and a band gap of ~0.7 eV. We demonstrate that the origin of the gap rests on band structure modifications induced by the CDW phase alone, without the need for Mott correlation effects. The results contribute towards the understanding and design of material platforms for memristors and low-energy devices in computing and data storage applications.

Authors: C.J. Sayers, G. Cerullo, Y. Zhang, C.E. Sanders, R.T. Chapman, A.S. Wyatt, G. Chatterjee, E. Springate, D. Wolverson, E. Da Como, E. Carpene

Contact author: E. Da Como
(edc25@bath.ac.uk)



(a) Illustration of the starlike lattice reconstruction in the CDW phase of 1T-TaSe₂. (b) Surface-projected Brillouin zone (BZ) of the undistorted “normal” state. The red dashed lines mimic the Fermi surface and the blue solid line indicates the experimental path through the BZ as measured by time- and angle-resolved photoemission spectroscopy (TR-ARPES) at Artemis (c) Sketch of the TR-ARPES experiment with laser photon energies.

Reproduced with permission from C.J. Sayers et al. *Phys. Rev. Lett.* 130, 156401 (2023)
© 2023 American Physical Society. doi:
10.1103/PhysRevLett.130.156401

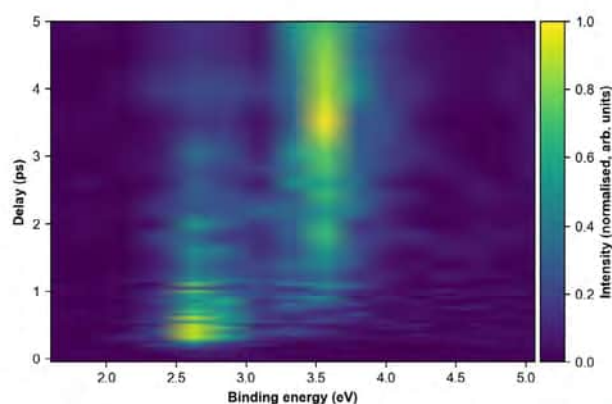
Ultrafast Rydberg-Valence Interactions and Photodissociation Dynamics of Trimethylamine: A Time-Resolved XUV Photoelectron Spectroscopy Experiment

The photodissociation dynamics of trimethylamine (TMA) have been studied using extreme ultraviolet (XUV) photoelectron spectroscopy. The XUV probe allows us to monitor the initial dynamics in the electronically excited Rydberg states, and how these correlate with the dissociation products formed.

Measurements show that following excitation into the 3p Rydberg state, competing internal conversion and dissociation processes occur leading to the 3p state lifetime of 4.4 ps. Dissociation directly from the 3p state leads to the formation of vibrationally hot methyl fragments in conjunction with ground state dimethyl amidogen (DMA), while internal conversion leads to population of the 3s Rydberg state. Once in the 3s state, the Rydberg state couples to a dissociative valence state leading to the formation of a vibrationally cold methyl radical and an electronically excited DMA on a 70 ps timescale.

Authors: D.J. Hughes, H.J. Thompson, R.S. Minns, P. Krüger, D.A. Horke, M.A. Parkes, R.T. Chapman, E. Springate, J.O.F. Thompson

Contact author: R.S. Minns
(r.s.minns@soton.ac.uk)



Time-resolved photoelectron spectrum of trimethylamine measured following excitation with a 6.1 eV pump and a 21.5 eV probe. The spectrum plotted highlights the initial Rydberg state dynamics involving internal conversion from the initially excited 3p Rydberg state, to the 3s Rydberg state.

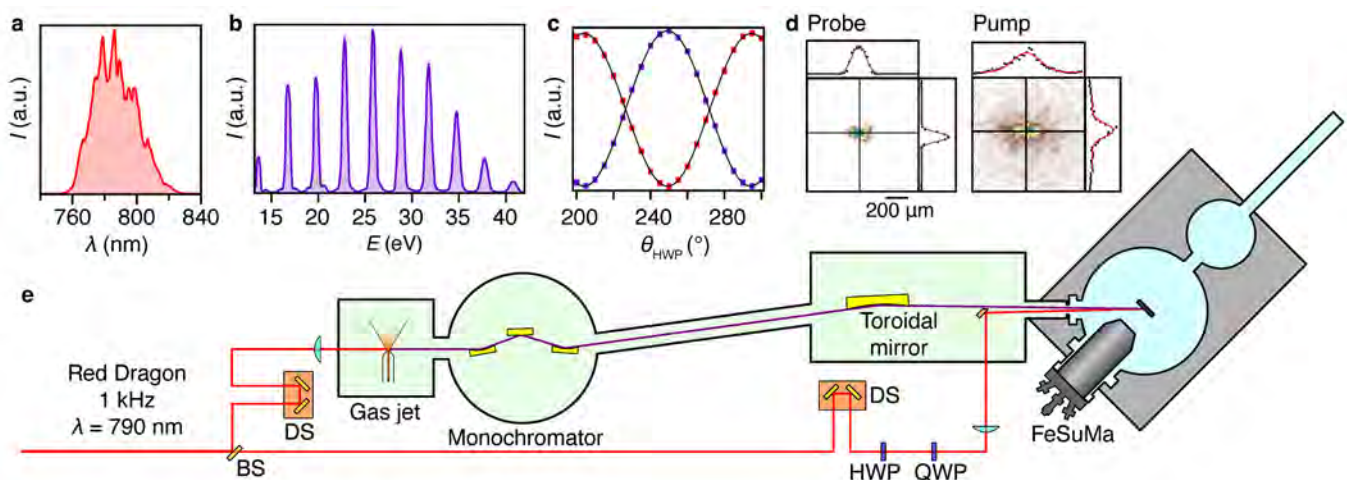
Access to the full three-dimensional Brillouin zone with time resolution, using a new tool for pump-probe photoemission spectroscopy

Artemis has reported on time- and angle-resolved photoemission spectroscopy (TR-ARPES) results that were acquired from solid-state samples using the new Fermiologics “FeSuMa” analyser. As the authors explain in their manuscript, which has recently been posted to the arXiv, the FeSuMa offers several advantages for TR-ARPES. The paper explores some of the ways in which the new analyser’s capabilities relate to those of hemispherical analysers and momentum microscopes. Artemis has integrated both the FeSuMa and a hemispherical analyser into a fully optimised pump-probe beamline that permits efficient photon-energy scanning for fully three-dimensional measurements, using probe energies generated from high harmonics in a gas jet. The advantages of using the FeSuMa in this situation include the possibility of taking advantage of its “fisheye” mode of operation.

Full information can be found in the manuscript, arXiv:2309.11535 [cond-mat.mtrl-sci], at <https://doi.org/10.48550/arXiv.2309.11535>

Authors: P. Majchrzak, P. Hofmann, A. Kuibarov, S. Borisenko, B. Büchner, Y. Zhang, R. Chapman, A. Wyatt, E. Springate, C.E. Sanders

Contact author: C.E. Sanders (charlotte.sanders@stfc.ac.uk)



(a) The spectrum of the 1-kHz titanium-sapphire (Ti:sapp) laser that was used to make the measurements reported in the new work. (b) The high-harmonics spectrum, driven by the Ti:sapp laser in an argon gas jet. (c) Calibration curves for pump polarisation, measured as intensity through a polariser after the beam passes through a quarter- and a half-wave plate (QWP and HWP, respectively). The intensity is shown as a function of rotation of the HWP. Control of the pump polarisation means that dichroic effects can be probed. (d) Spot sizes of the probe and pump beams. (e) Schematic of the experimental setup. “DS” indicates “delay stage.” “BS” indicates a beam splitter.

Reproduced from C.E. Sanders et al. arxiv.org/abs/2309.11535 [cond-mat.mtrl-sci], under the terms of the [Creative Commons Attribution 4.0 licence](https://creativecommons.org/licenses/by/4.0/) doi:10.48550/arXiv.2309.11535

The guidance and adhesion protein FLRT2 dimerizes in *cis* via dual small- X_3 -small transmembrane motifs

Fibronectin Leucine-rich Repeat Transmembrane (FLRT 1–3) proteins are a family of broadly expressed single-spanning transmembrane receptors that play key roles in development. Their extracellular domains mediate homotypic cell-cell adhesion and heterotypic protein interactions with other receptors to regulate cell adhesion and guidance. These *in trans* FLRT interactions determine the formation of signaling complexes of varying complexity and function. Whether FLRTs also interact at the surface of the same cell, *in cis*, remains unknown. Here, molecular dynamics simulations reveal two dimerization motifs in the FLRT2 transmembrane helix. Single particle tracking experiments show that these Small- X_3 -Small motifs synergize with a third dimerization motif encoded in the extracellular domain to permit the *cis* association and co-diffusion patterns of FLRT2 receptors on cells. These results may point to a competitive switching mechanism between *in cis* and *in trans* interactions, which suggests that homotypic FLRT interaction mirrors the functionalities of classic adhesion molecules.

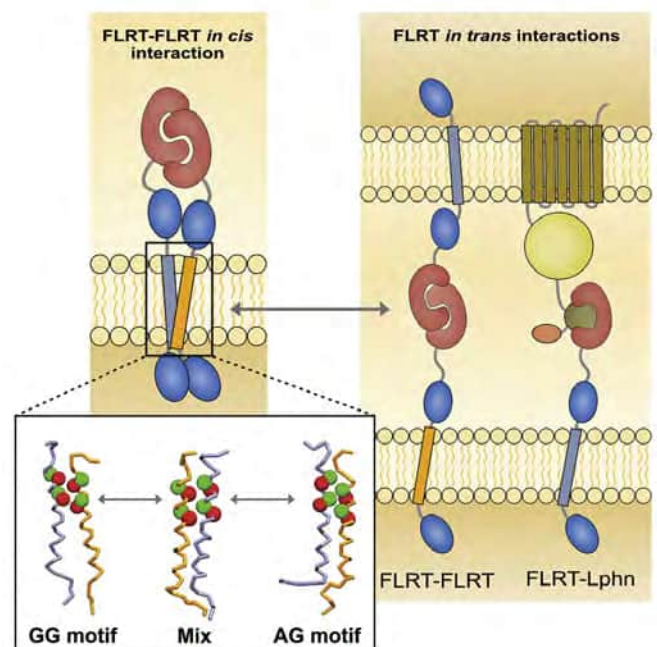
Reproduced from Jackson, V. et al. (2022). *The guidance and adhesion protein FLRT2 dimerizes in cis via dual small- X_3 -small transmembrane motifs*. *Structure* 30, 1354–1365.e5 © Elsevier Ltd under an [Elsevier user license](#). doi: 10.1016/j.str.2022.05.014

Authors: V. Jackson, R.A. Corey, A.L. Duncan, A. Chu, M.S.P. Sansom, E. Seiradake, J. Hermann, C.J. Tynan, D.J. Rolfe, M.L. Martin-Fernandez, M. Noriega, M. Chavent, A.C. Kalli, E.Y. Jones

Contact authors: M.L. Martin-Fernandez (marisa.martin-fernandez@stfc.ac.uk)

E. Seiradake (elena.sieradake@bioch.ox.ac.uk)

M. Chavent (matthieu.chavent@ipbs.fr)



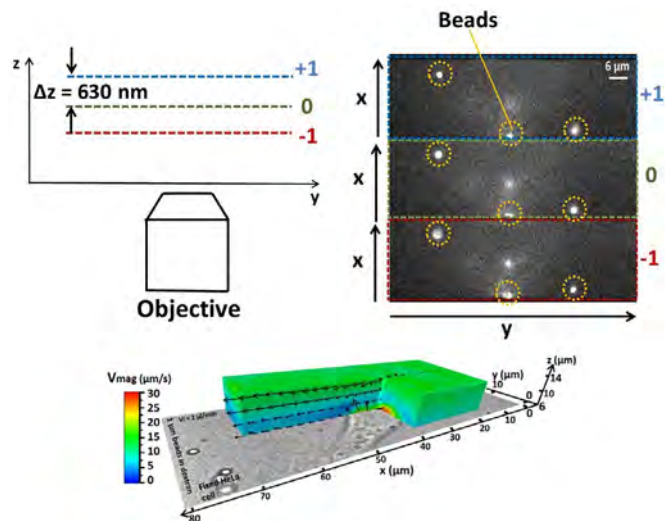
Instantaneous 4D micro-particle image velocimetry (μ PIV) via multifocal microscopy (MUM)

Multifocal microscopy (MUM), a technique to capture multiple fields of view (FOVs) from distinct axial planes simultaneously and on one camera, was used to perform micro-particle image velocimetry (μ PIV) to reconstruct velocity and shear stress fields imposed by a liquid flowing around a cell. A diffraction based multifocal relay was used to capture images from three different planes with 630 nm axial spacing from which the axial positions of the flow-tracing particles were calculated using the image sharpness metric. It was shown that MUM can achieve an accuracy on the calculated velocity of around $(0.52 \pm 0.19) \mu\text{m/s}$. Using fixed cells, MUM imaged the flow perturbations at subcellular level, which showed characteristics similar to those observed in the literature. Using live cells as an exemplar, MUM observed the effect of changing cell morphology on the local flow during perfusion. Compared to standard confocal laser scanning microscope, MUM offers a clear advantage in acquisition speed for μ PIV (over 300 times faster). This is an important characteristic for rapidly evolving biological systems where there is the necessity to monitor in real time entire volumes to correlate the sample responses to the external forces.

Reproduced from Guastamacchia, M.G.R., Xue, R., Madi, K. et al. Instantaneous 4D micro-particle image velocimetry (μ PIV) via multifocal microscopy (MUM). Sci Rep 12, 18458 (2022) under the term of a [Creative Commons Attribution 4.0 International License](#). doi:10.1038/s41598-022-22701-3

Authors: M.G.R. Guastamacchia, W.T.E. Pitkeathly, P.A. Dalgarno, R. Xue, P.D. Lee, S.H. Cartmell, K. Madi, S.E.D. Webb

Contact author: P.A. Dalgarno (p.a.dalgarno@hw.ac.uk)



Top panels: In multifocal fluorescence microscopy, images of different axial planes of the same area are collected simultaneously in different regions of a single camera. For this paper, we used a diffraction grating that placed the planes 630 nm apart. The differing sharpness of an object within the three sub-images is used to determine its axial position, with fluorescent beads used to calibrate the microscope.

Bottom panel: By acquiring a time series of images of fluorescent beads flowing over a cell, the magnitude (colour) and direction (arrows) of bead velocities can be mapped in 3D. Here, we used 1 μm beads in dextran flowing over a fixed HeLa cell to image the cell-induced perturbation of the flow. The white light transmission image of the cell was collected using a second camera via an image splitter.

Ultraviolet refractive index values of organic aerosol extracted from deciduous forestry, urban and marine environments

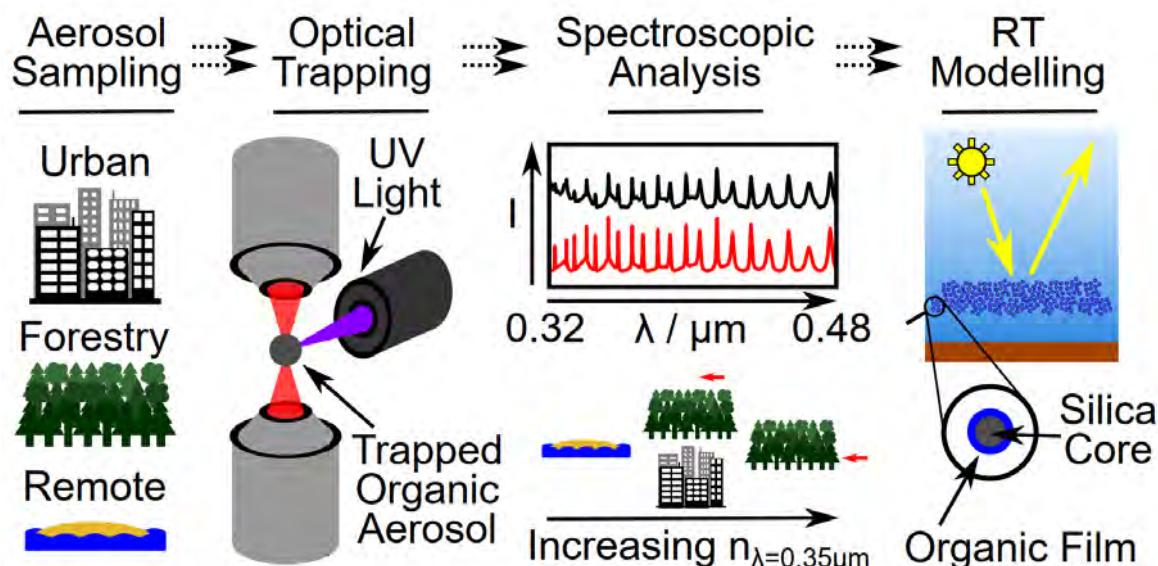
The refractive index values of atmospheric aerosols are required to address the large uncertainties in the magnitude of atmospheric radiative forcing and measurements of the refractive index dispersion with wavelength of particulate matter sampled from the atmosphere are rare over ultraviolet wavelengths. An ultraviolet-optimized spectroscopic system illuminates optically-trapped single particles from a range of tropospheric environments to determine the particle's optical properties. Aerosol from remote marine, polluted urban, and forestry environments is collected on quartz filters, and the organic fraction is extracted and nebulized to form micron-sized spherical particles. The radius and the real component of refractive index dispersion with wavelength of the optically trapped particles are determined to a precision of 0.001 μm and 0.002 respectively over a near-ultraviolet-visible wavelength range of 0.320–0.480 μm . Remote marine aerosol is observed to have the lowest refractive index ($n = 1.442$ ($\lambda = 0.350 \mu\text{m}$)), with above-canopy rural forestry aerosol ($n = 1.462$ – 1.481 ($\lambda = 0.350 \mu\text{m}$)) and polluted urban aerosol ($n = 1.444$ – 1.485 ($\lambda = 0.350 \mu\text{m}$)) showing similar refractive index dispersions with wavelength.

In-canopy rural forestry aerosol is observed to have the highest refractive index value ($n = 1.508$ ($\lambda = 0.350 \mu\text{m}$)). The study presents the first single particle measurements of the dispersion of refractive index with wavelength of atmospheric aerosol samples below wavelengths of 0.350 μm . The Cauchy dispersion equation, commonly used to describe the visible refractive index variation of aerosol particles, is demonstrated to extend to ultraviolet wavelengths below 0.350 μm for the urban, forestry, and atmospheric aerosol water-insoluble extracts from these environments. A 1D radiative-transfer calculation of the difference in top-of-the-atmosphere albedo between atmospheric core-shell mineral aerosol with and without films of this material demonstrates the importance of organic films forming on mineral aerosol.

Reproduced from *Environ. Sci.: Atmos.*, 2023,3, 1008-1024, under the terms of a [Creative Commons Attribution 3.0 Unported licence](https://creativecommons.org/licenses/by/3.0/).
doi: 10.1039/d3ea00005b

Authors: C.R. Barker, E.J. Stuckey, M.L. Poole, M.D. King, M. Wilkinson, J. Morison, A. Wilson, G. Little, R.J.L. Welbourn, A.D. Ward

Contact author: M.D. King (m.king@rhul.ac.uk)



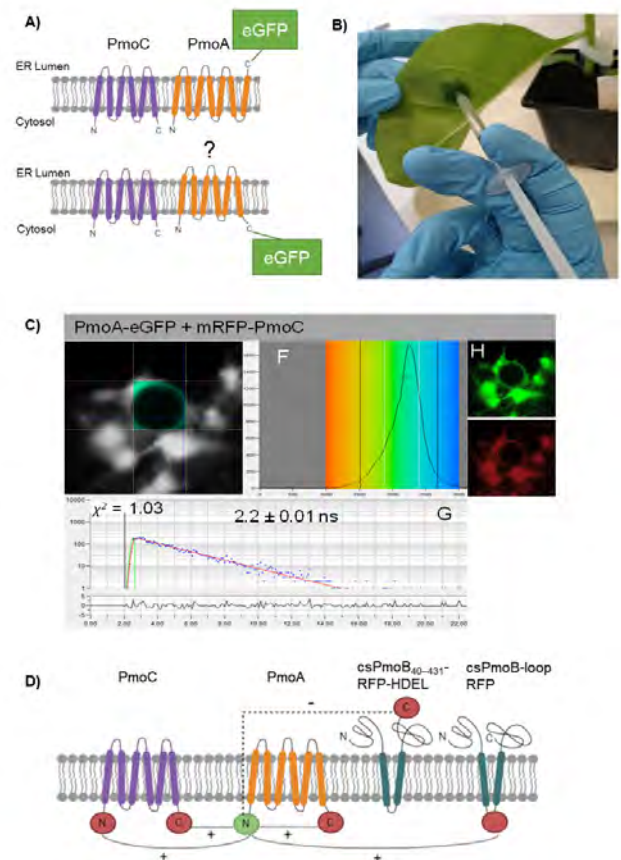
FRET-FLIM to determine protein interactions and membrane topology of enzyme complexes

Determining protein-protein interactions is vital for gaining knowledge on cellular and metabolic processes including enzyme complexes and metabolons. Förster resonance energy transfer with fluorescence lifetime imaging microscopy (FRET-FLIM) is an advanced imaging methodology that allows for the quantitative detection of protein-protein interactions. In this method, proteins of interest for interaction studies are fused to different fluorophores such as enhanced green fluorescent protein (eGFP; donor molecule) and monomeric red fluorescent protein (mRFP; acceptor molecule). Energy transfer between the two fluorophore groups can only occur efficiently when the proteins of interest are in close physical proximity, around ≤ 10 nm, and therefore are most likely interacting. FRET-FLIM measures the decrease in excited-state lifetime of the donor fluorophore (eGFP) with and without the presence of the acceptor (mRFP) and can therefore give information on protein-protein interactions and the membrane topology of the tested protein. Here we describe the production of fluorescent protein fusions for FRET-FLIM analysis in tobacco leaf epidermal cells using *Agrobacterium*-mediated plant transformation and a FRETFLIM data acquisition and analysis protocol in plant cells. These protocols are applicable and can be adapted for both membrane and soluble proteins in different cellular localizations.

Reproduced from Spatola Rossi, T., Pain, C., Botchway, S. W., & Kriechbaumer, V. (2022). FRET-FLIM to determine protein interactions and membrane topology of enzyme complexes. Current Protocols, 2, e598, under the terms of a [Creative Commons Attribution License](https://creativecommons.org/licenses/by/4.0/). doi: 10.1002/cpz1.598

Authors: V. Kriechbaumer, T.S. Rossi, C. Pain, S.W. Botchway

Contact author: V. Kriechbaumer (vkriechbaumer@brookes.ac.uk)



FRET-FLIM interactions can resolve membrane topologies: the bacterial pMMO enzyme complex as an example. (A) Schematic diagram of topology predictions for the enzymes PmoC and PmoA. PmoC is predicted to feature six TMDs. Predictions for PmoA differ between six and seven TMDs, and the C-terminus could therefore either face the ER lumen (top) or the cytosol (bottom). (B) Agrobacterium-mediated tobacco leaf infiltration is carried out to produce the proteins in planta with fluorescent tags. (C) FRET-FLIM analysis is carried out, here as an example PmoA-eGFP with mRFP-PmoC. Different combinations reveal that PmoA features 6 TMDs with both termini in the cytosol.

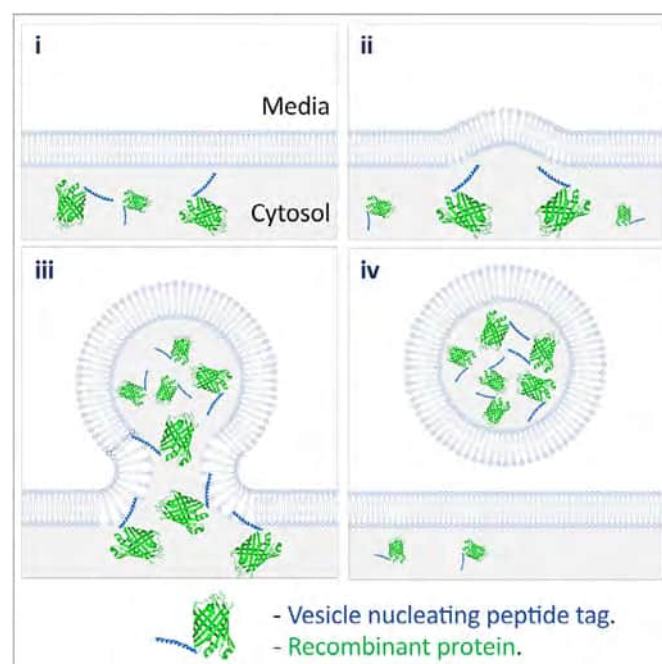
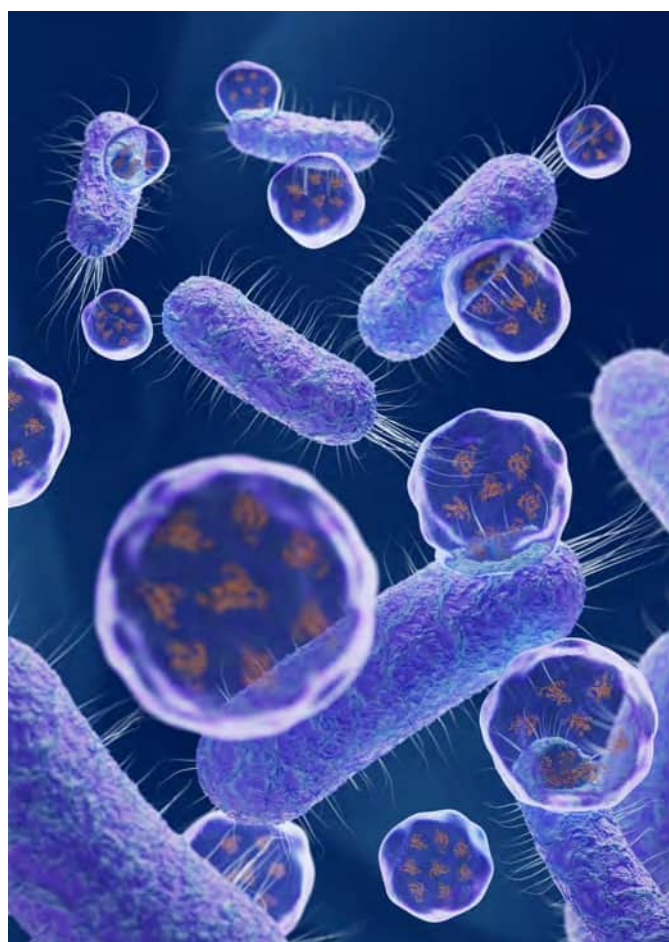
High-yield vesicle-packaged recombinant protein production from *E. coli*

We describe an innovative system that exports diverse recombinant proteins in membrane-bound vesicles from *E. coli*. These recombinant vesicles compartmentalize proteins within a micro-environment that enables production of otherwise challenging insoluble, toxic, or disulfide-bond containing proteins from bacteria. The release of vesicle-packaged proteins supports isolation from the culture and allows long-term storage of active protein. This technology results in high yields of vesicle-packaged, functional proteins for efficient downstream processing for a wide range of applications from discovery science to applied biotechnology and medicine.

Reproduced from Eastwood, Tara A et al. "High-yield vesicle-packaged recombinant protein production from *E. coli*." *Cell Reports Methods* 3, 100396, 2023, doi: under the terms of a [Creative Commons Attribution License](#). doi: 10.1016/j.crmeth.2023.100396

Authors: T.A. Eastwood, K. Baker, B.R. Streather, I.R. Brown, D.P. Mulvihill, N. Allen, L. Wang, S.W. Botchway, J.R. Hiscock, C. Lennon

Contact author: D.P. Mulvihill (d.p.mulvihill@kent.ac.uk)



A simple peptide tag generates recombinant-protein-filled vesicles from *E. coli*. This approach allows simplified production of recombinant protein at high yields.

Microsphere-supported gold nanoparticles for SERS detection of malachite green

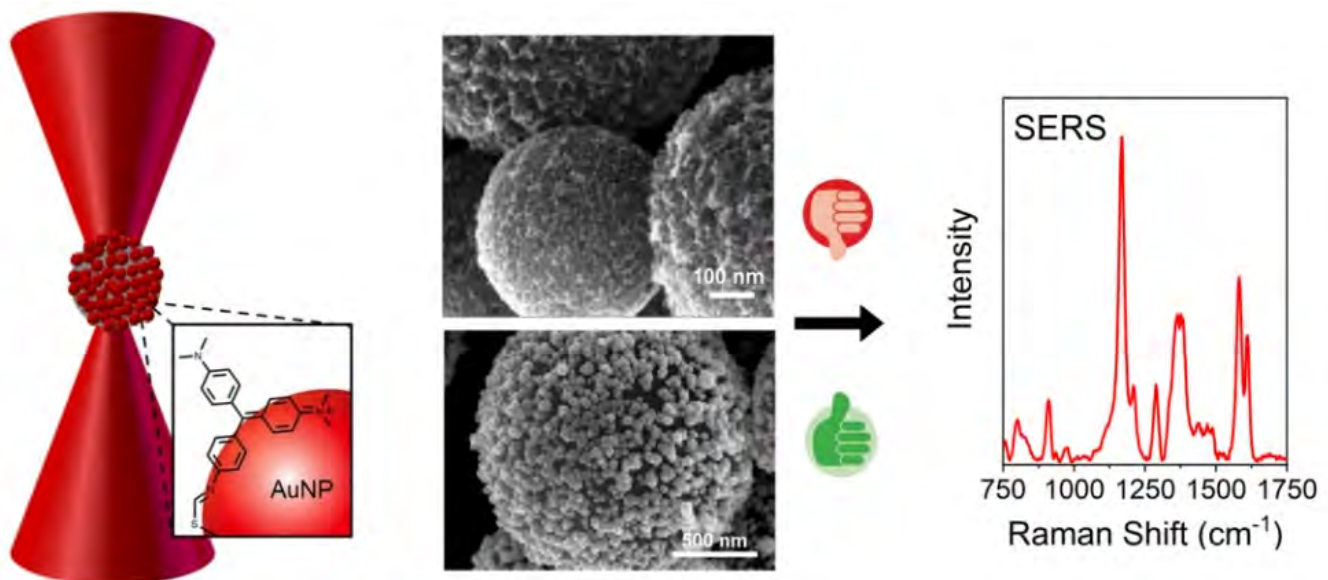
Supported metal nanoparticles are attractive for wide ranging applications including catalysis and imaging. In this work we prepare surface-enhanced Raman scattering (SERS) active materials by exploiting the high surface area of porous carbon microspheres (C_μP) to assemble high loadings of gold nanoparticles (AuNPs). The specific surface functionalization of C_μP is exploited to prepare composites by two approaches, (1) carboxylic acid surface groups are used to attract positively charged AuNPs and (2) a thiol functionalized surface is used to immobilize AuNPs. Ripening of the surface immobilized gold nanoparticles through hydroquinone treatment results in the preparation of a roughened gold surface with a 22-fold increase in the Au loading from 0.3 to 7.0 (mass Au/mass C). The materials were thoroughly characterized by UV-vis, Infrared and Raman spectroscopy, DLS, zeta potential, TEM and SEM.

The SERS capacity of individual particles to detect malachite green, a mutagenic fungicide used in fish farming, was investigated using Raman optical tweezers. The challenges to trapping these materials due to the significant reflection, refraction and scattering properties of the Au-coated surfaces was overcome using a pinning approach. The measurements revealed the detection of malachite green at nM concentration and showed the potential of the porous carbon particles to act as versatile scaffolds for SERS applications.

Reproduced from D. T. Hinds, S. A. Belhout, P. E. Colavita, A. D. Ward and S. J. Quinn, *Mater. Adv.*, 2023, 4, 1481, under the terms of a [Creative Commons Attribution 3.0 Unported License](https://creativecommons.org/licenses/by/3.0/). doi: 10.1039/D2MA00997H

Authors: D.T. Hinds, P.E. Colavita, S.J. Quinn, S.A. Belhout, A.D. Ward

Contact author: S.J. Quinn
(susan.quinn@ucd.ie)



A porous carbon microsphere decorated with gold nanoparticles has been shown to act as a sensitive SERS substrate for the detection of malachite green. The use of an optical trap allows exclusive probing of individual composite particles and reveals the impact of the roughened gold surface on detection.

From Chemotherapy to Phototherapy – Changing the Therapeutic Action of a Metallo-Intercalating Ru^{II}-Re^I Luminescent System by Switching its Sub-Cellular Location

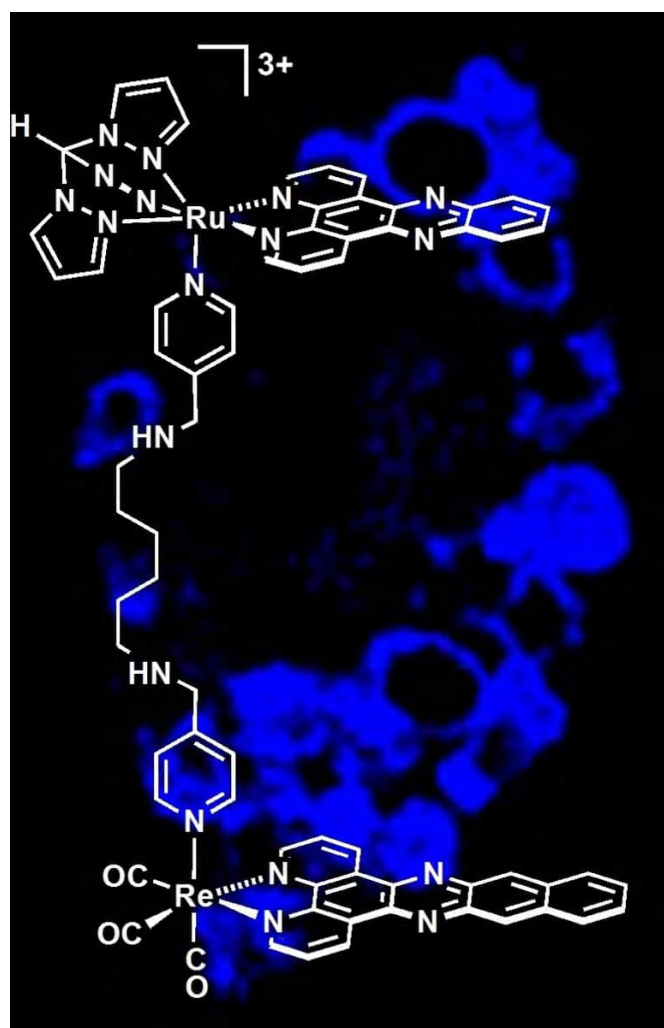
The synthesis of a new heterodinuclear Re^IRu^{II} metallointercalator containing Ru^{II}(dppz) and Re^I(dppn) moieties is reported. Cell-free studies reveal that the complex has similar photophysical properties to its homoleptic M(dppz) analogue and it also binds to DNA with a similar affinity. However, the newly reported complex has very different in-cell properties to its parent. In complete contrast to the homoleptic system, the Ru^{II}(dppz)/Re^I(dppn) complex is not intrinsically cytotoxic but displays appreciable phototoxic, despite both complexes displaying very similar quantum yields for singlet oxygen sensitization. Optical microscopy suggests that the reason for these contrasting biological effects is that whereas the homoleptic complex localises in the nuclei of cells, the Ru^{II}(dppz)/Re^I(dppn) complex preferentially accumulates in mitochondria. These observations illustrate how even small structural changes in metal based therapeutic leads can modulate their mechanism of action.

Reproduced from *Chem. Eur. J.* 2023, **29**, e202300617, under the terms of a [Creative Commons Attribution License](https://creativecommons.org/licenses/by/4.0/). doi: 10.1002/chem.202300617

Authors: H.K. Saeed, A.J. Auty, A.A.P. Chauvet, J.A. Thomas, P.J. Jarman, R. Mowll, C.G.W. Smythe, S. Sreedharan, J. Bernardino de la Serna

Contact authors: J.A. Thomas (james.thomas@sheffield.ac.uk)

J. Bernardino de la Serna (j.bernardino-de-la-serna@imperial.ac.uk)



Binding partners regulate unfolding of myosin VI to activate the molecular motor

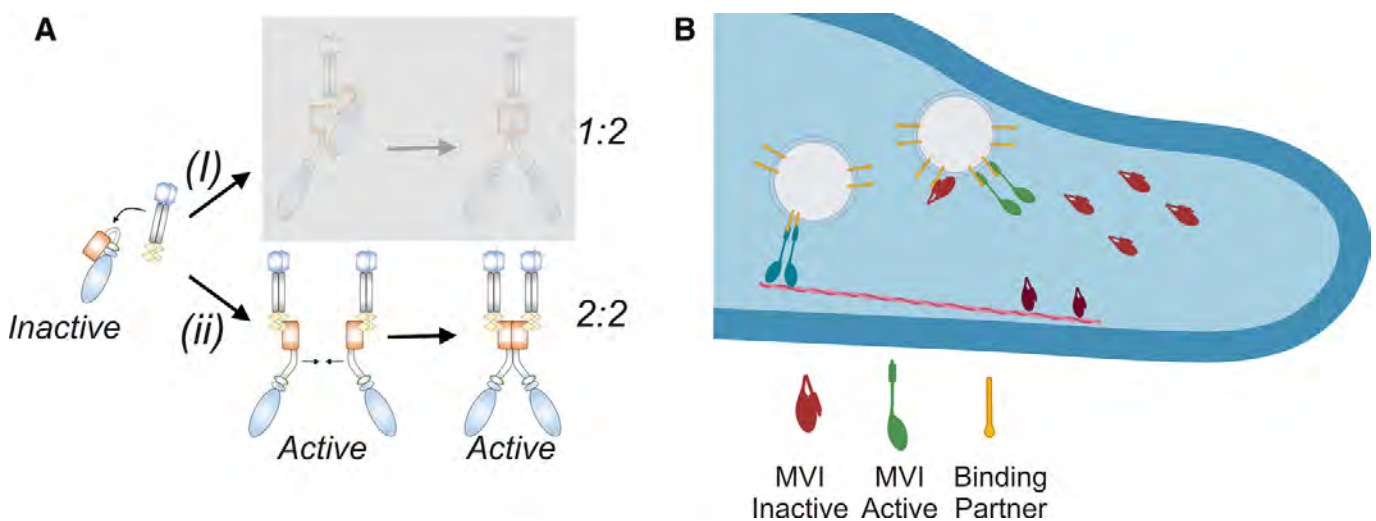
Myosin VI is the only minus-end actin motor and it is coupled to various cellular processes ranging from endocytosis to transcription. This multi-potent nature is achieved through alternative isoform splicing and interactions with a network of binding partners. There is a complex interplay between isoforms and binding partners to regulate myosin VI. Here, we have compared the regulation of two myosin VI splice isoforms by two different binding partners. By combining biochemical and single-molecule approaches, we propose that myosin VI regulation follows a generic mechanism, independently of the spliced isoform and the binding partner involved. We describe how myosin VI adopts an autoinhibited backfolded state which is released by binding partners. This unfolding activates the motor, enhances actin binding and can subsequently trigger dimerization.

We have further expanded our study by using single-molecule imaging to investigate the impact of binding partners upon myosin VI molecular organization and dynamics.

Reproduced from Dos Santos Á, Fili N, Hari-Gupta Y, et al. Binding partners regulate unfolding of myosin VI to activate the molecular motor. Biochem J. 2022;479(13):1409-1428, published by Portland Press Limited, under the terms of a [Creative Commons Attribution 4.0 International License](https://creativecommons.org/licenses/by/4.0/). doi:10.1042/BCJ20220025

Authors: Á. dos Santos, N. Fili, R.E. Gough, C.P. Toseland, Y. Hari-Gupta, L. Wang, M. Martin-Fernandez, J. Aaron, E. Wait, T-L, Chew

Contact author: C.P. Toseland (c.toseland@sheffield.ac.uk)



Model describing the activation of myosin VI by binding partners. (A) Two routes of binding partner dependent dimerization of MVI. (B) Recruitment and activation of myosin VI to cellular cargo by binding partners.

Structure and activity of particulate methane monooxygenase arrays in methanotrophs

Methane-oxidizing bacteria play a central role in greenhouse gas mitigation and have potential applications in biomanufacturing. Their primary metabolic enzyme, particulate methane monooxygenase (pMMO), is housed in copper-induced intracytoplasmic membranes (ICMs), of which the function and biogenesis are not known. We show by serial cryo-focused ion beam (cryoFIB) milling/scanning electron microscope (SEM) volume imaging and lamellae-based cellular cryo-electron tomography (cryoET) that these ICMs are derived from the inner cell membrane. The pMMO trimer, resolved by cryoET and subtomogram averaging to 4.8 Å in the ICM, forms higher-order hexagonal arrays in intact cells. Array formation correlates with increased enzymatic activity, highlighting the importance of studying the enzyme in its native environment. These findings also demonstrate the power of cryoET to structurally characterize native membrane enzymes in the cellular context.

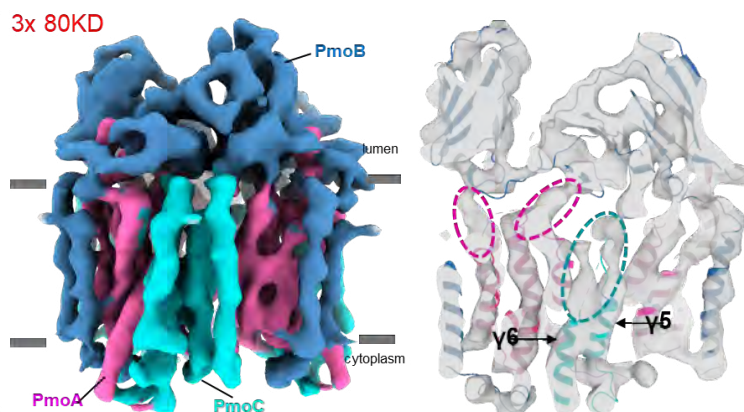
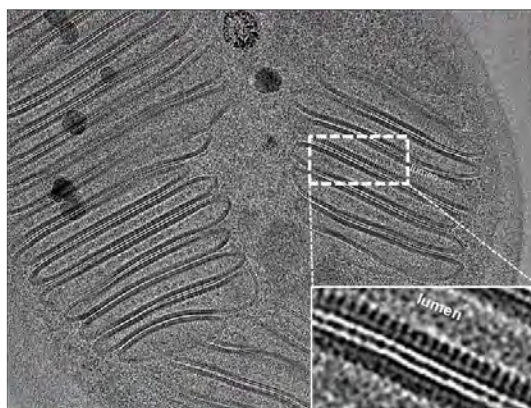
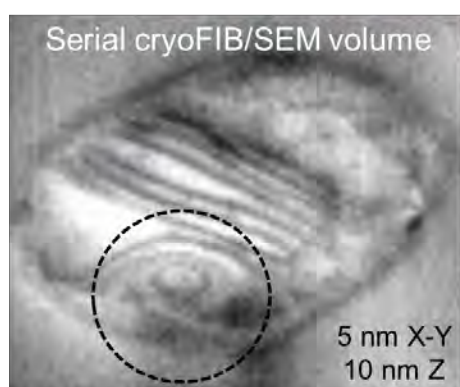
Reproduced from Zhu, Y., Koo, C.W., Cassidy, C.K. et al. Structure and activity of particulate methane monooxygenase arrays in methanotrophs. *Nat Commun* 13, 5221 (2022), under the term of a [Creative Commons Attribution 4.0 International License](https://creativecommons.org/licenses/by/4.0/). doi: 10.1038/s41467-022-32752-9

Authors: Y. Zhu, T. Ni, J. Shen, C.W. Koo, A.C. Rosenzweig, C.K. Cassidy, M.C. Spink, Y. Sheng, Y. Song, Z. Yang, L.C. Zanetti-Domingues, B.C. Bateman, M. L. Martin-Fernandez, P. Zhang

Contact authors: A.C. Rosenzweig (amyrr@northwestern.edu)

P. Zhang (peijun.zhang@strubi.ox.ac.uk)

CryoET STA of pMMO structure at 4.8 Å



Kerr-gated Raman investigations to understand LDPE decomposition by zeolites

This work uses an optical time gating technique to collect Raman spectra during the catalytic conversion of low-density polyethylene on different zeolites. The chemical recycling of “non-recyclable” plastics is an important step towards a circular carbon economy.

In applying Raman spectroscopy during plastic conversion, we can relate spectral changes with the catalytic activity, to understand further our separately collected catalytic testing data. Intermediate species have been identified, and primary decomposition is separated from secondary reactions taking place, for example to give aromatic side products. Studying such a system under real operando conditions up to 400°C in temperature is extremely challenging, but thanks to the Kerr-gated spectrometer, we can reject fluorescence that otherwise interferes with the Raman signals being collected.

The work highlights zeolite characteristics that are the most and least useful for the process of LDPE pyrolysis, for conversion back to pyrolysis oils for the synthesis of new virgin-grade plastic.

Authors: E. Campbell, S. Wallbridge, S. Dann, S. Kondrat, I. V. Sazanovich, P. Moreau, A. M. Beale

Contact author: E. Campbell
(Campbelle3@cardiff.ac.uk)

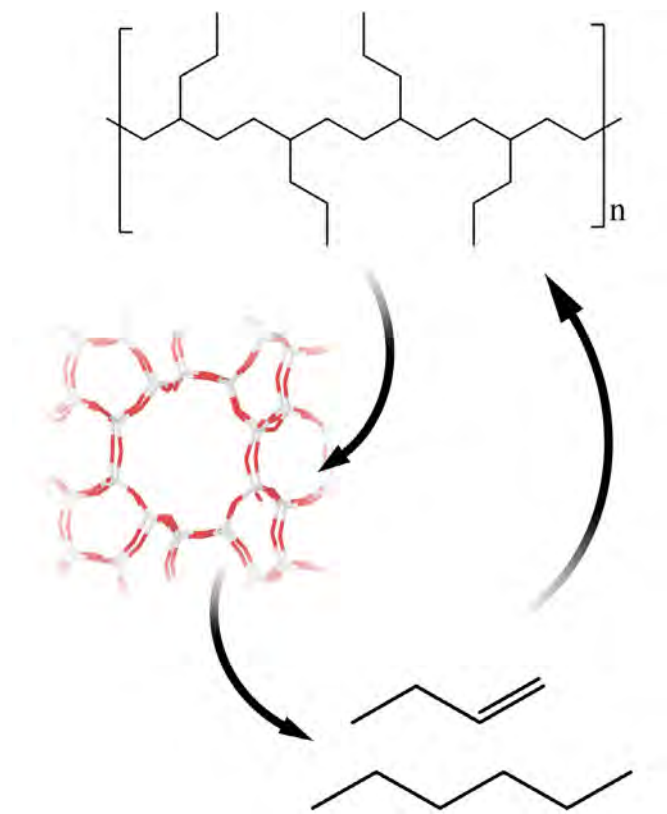


Figure 1: Figure of circularity of the process of chemically recycling LDPE with zeolite catalyst

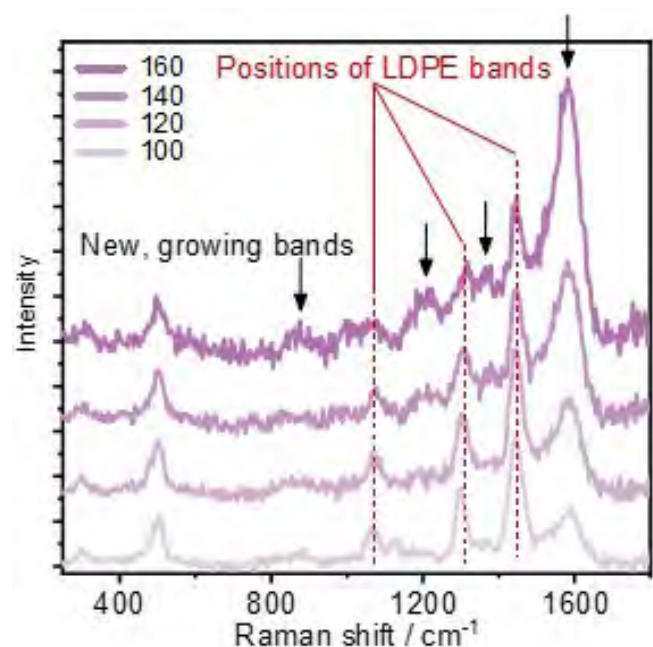


Figure 2: Raman spectra collected during the conversion of LDPE using H-Y as a catalyst

Time-Resolved Resonance Raman Spectroscopy of a Water Splitting Photocatalyst

We have reported new Kerr-gated Time-resolved Raman (TR^3) data for the linear polymer photocatalyst P10, and identified a new strong Raman mode of the P10 electron polaron. Interestingly experiments with P10 samples loaded with an IrO_x water oxidation catalyst also show clear evidence for long-lived electrons. The photoelectrons generated persist for >1 ns with no clear changes in the Raman spectra, indicating that electron transfer to the catalytic sites of hydrogen evolution is slow and further slow TR^3 studies could explore this potential kinetic bottleneck.

Authors: C. Li, O. Thwaites, A.M. Gardner, I.V. Sazanovich, A.J. Cowan

Contact author: A.J. Cowan
(acowan@liverpool.ac.uk)

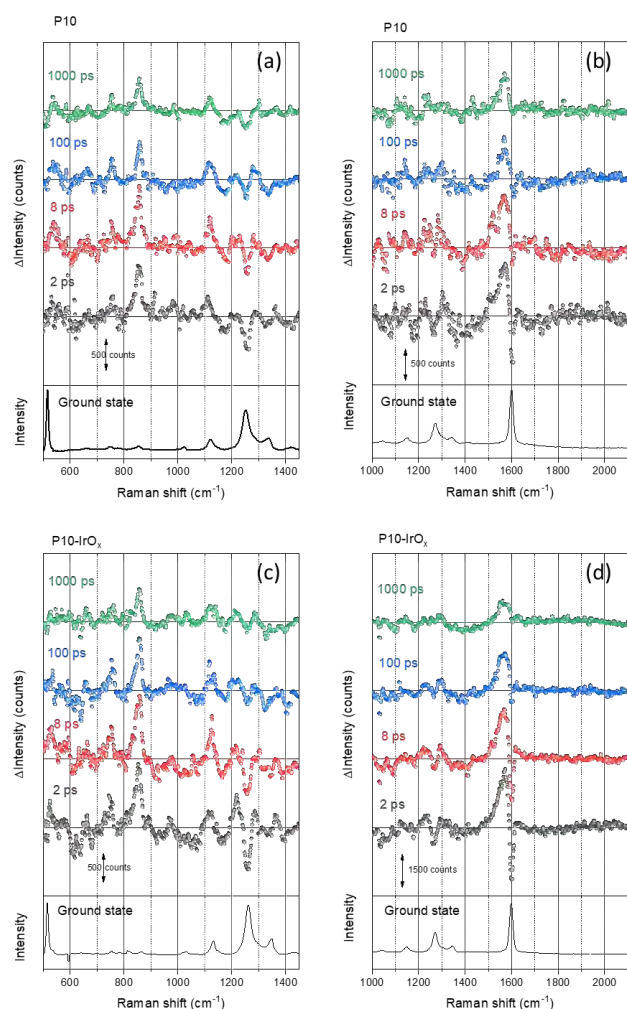


Figure 1: Kerr gated TR^3 spectra and ground state spectra (all 630 nm probe) recorded of P10 and P10- IrO_x following 400 nm excitation

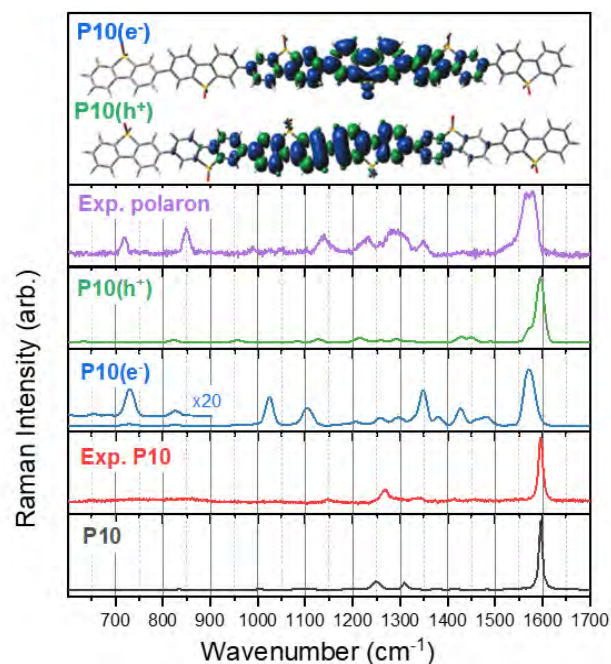


Figure 2: Density functional theory (DFT) calculated spectra and schematic of polaron localisation on a P10 hexamer (theory level $\omega\text{B97XD/cc-pVDZ}$). Also included is a P10 polaron (electron) recorded under steady state illumination conditions

Figure 2 reproduced from *J. Phys. Chem. Lett.* 2021, 12, 10899–10905, under the terms of the [Creative Commons CC-BY 4.0 License](https://creativecommons.org/licenses/by/4.0/). doi: 10.1021/acs.jpcllett.1c03073

Laser induced temperature-jump time resolved IR spectroscopy of zeolites

Combining pulsed laser heating and time-resolved infrared (TR-IR) absorption spectroscopy provides a means of initiating and studying thermally activated chemical reactions and diffusion processes in heterogeneous catalysts on timescales from nanoseconds to seconds. To this end, we investigated single pulse and burst laser heating in zeolite catalysts under realistic conditions using TR-IR spectroscopy. 1 ns, 70 μJ , 2.8 μm laser pulses from a Nd:YAG-pumped optical parametric oscillator were observed to induce temperature-jumps (T-jumps) in zeolite pellets in nanoseconds, with the sample cooling over 1 – 3 ms. By adopting a tightly focused beam geometry, T-jumps as large as 145°C from the starting temperature were achieved, demonstrated through comparison of the TR-IR spectra with temperature dependent IR absorption spectra and three dimensional heat transfer modelling using realistic experimental parameters. The simulations provide a detailed understanding of the temperature distribution within the sample and its evolution over the cooling period, which we observe to be bi-exponential. These results provide foundations for determining the magnitude of a T-jump in a catalyst/adsorbate system from its absorption spectrum and physical properties, and for applying T-jump TR-IR spectroscopy to the study of reactive chemistry in heterogeneous catalysts.

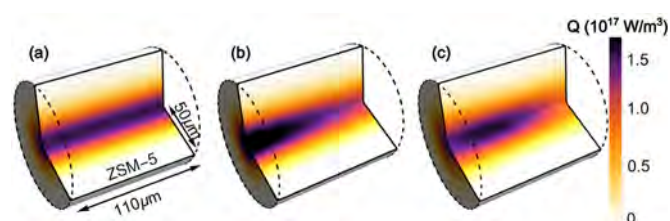


Figure 1: 3D distribution of heat supplied by the pump laser in heat transfer simulations, showing in sequence: (a) a Gaussian pump beam passing unattenuated through the sample; (b) the added effect of attenuation of the pump as it passes through the sample; (c) the added effect of the divergence of the pump beam.

Reproduced from Hawkins AP, Edmeades AE, Hutchison CDM, Towrie M, Howe RF, Greetham GM, et al., Laser induced temperature-jump time resolved IR spectroscopy of zeolites, ChemRxiv 2023, under the terms of a [Creative Commons CC BY 4.0 License](https://creativecommons.org/licenses/by/4.0/). doi:10.26434/chemrxiv-2023-p5gsr. The content is a preprint and has not been peer-reviewed.

Authors: A.P. Hawkins, A.E. Edmeades, C.D.M. Hutchison, M. Towrie, R.F. Howe, G.M. Greetham, P.M. Donaldson

Contact authors: A.P. Hawkins (alex.hawkins@stfc.ac.uk)

P.M. Donaldson (paul.donaldson@stfc.ac.uk)

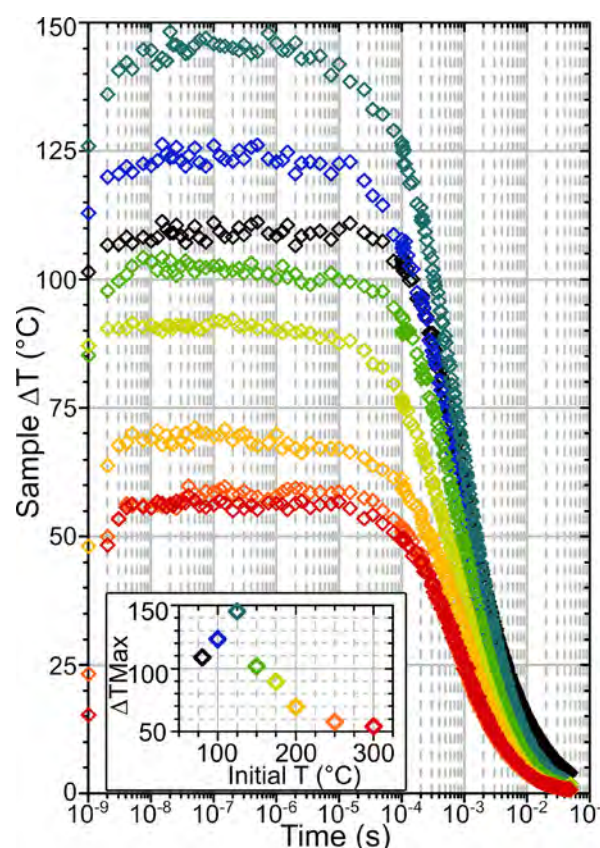


Figure 2: Sample heating vs time after ns laser heating for HOD/H₂O dosed ZSM-5, at different initial temperatures calculated based on changes in silanol mode intensity. The inset plot shows the maximum ΔT achieved against initial temperature. The colour scheme of the heating transients corresponds to that in the inset.

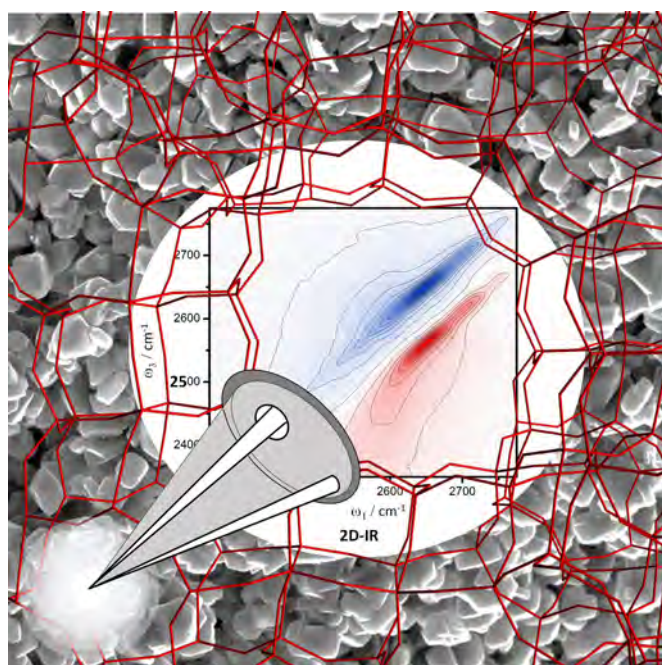
Ultrafast 2D-IR spectroscopy of intensely optically scattering pelleted solid catalysts

Solid, powdered samples are often prepared for infrared (IR) spectroscopy analysis in the form of compressed pellets. The intense scattering of incident light by such samples inhibits applications of more advanced IR spectroscopic techniques, such as two-dimensional (2D)-IR spectroscopy. We describe here an experimental approach that enables the measurement of high-quality 2D-IR spectra from scattering pellets of zeolites, titania, and fumed silica in the OD-stretching region of the spectrum under flowing gas and variable temperature up to $\sim 500^\circ\text{C}$. In addition to known scatter suppression techniques, such as phase cycling and polarization control, we demonstrate how a bright probe laser beam comparable in strength with the pump beam provides effective scatter suppression. The possible nonlinear signals arising from this approach are discussed and shown to be limited in consequence. In the intense focus of 2D-IR laser beams, a free-standing solid pellet may become elevated in temperature compared with its surroundings. The effects of steady state and transient laser heating effects on practical applications are discussed.

Reproduced from *J. Chem. Phys.* 158, 114201 (2023), under the terms of a [Creative Commons CC BY 4.0 License](https://creativecommons.org/licenses/by/4.0/). doi: 10.1063/5.0139103

Authors: P.M. Donaldson, R.F. Howe, A.P. Hawkins, M. Towrie, G.M. Greetham

Contact author: P.M. Donaldson (paul.donaldson@stfc.ac.uk)



Zeolites are microcrystalline heterogeneous catalysts with nanometre scale pores, as shown in the superimposed SEM image and crystal structure. In this figure, a 2D-IR spectrum of zeolite Y is drawn in the zeolite pore. Measurement of spectra such as these was enabled by new methods developed to reject the intense optical scatter of the samples.

Spectrophotometric Concentration Analysis Without Molar Absorption Coefficients by Two-Dimensional-Infrared and Fourier Transform Infrared Spectroscopy

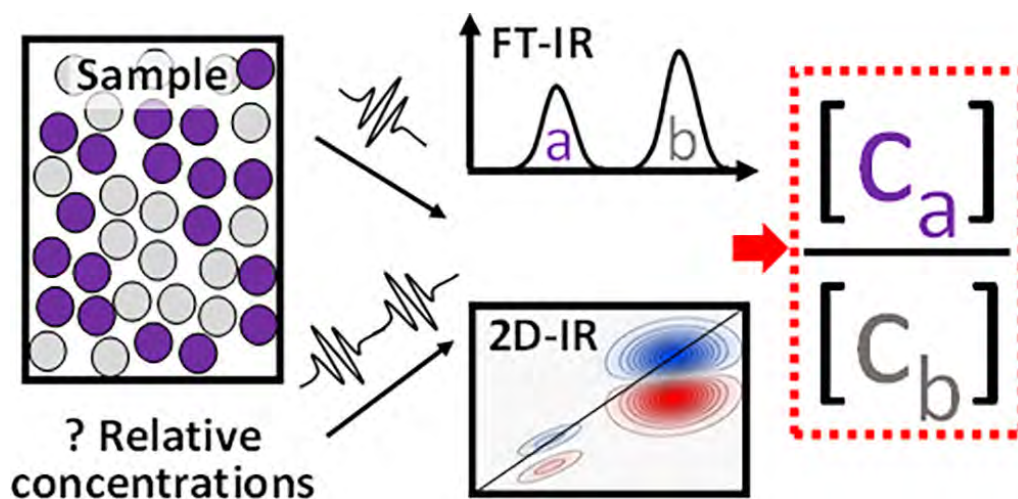
A spectrophotometric method for determining relative concentrations of infrared (IR)-active analytes with unknown concentration and unknown molar absorption coefficient is explored. This type of method may be useful for the characterization of complex/heterogeneous liquids or solids, the study of transient species, and for other scenarios where it might be difficult to gain concentration information by other means. Concentration ratios of two species are obtained from their IR absorption and two-dimensional (2D)-IR diagonal bleach signals using simple ratiometric calculations. A simple calculation framework for deriving concentration ratios from spectral data is developed, extended to IR-pump-probe signals, and applied to the calculation of transition dipole ratios. Corrections to account for the attenuation of the 2D-IR signal caused by population relaxation, spectral overlap, wavelength-dependent pump absorption, inhomogeneous broadening, and laser intensity variations are described.

A simple formula for calculating the attenuation of the 2D-IR signal due to sample absorption is deduced and by comparison with 2D-IR signals at varying total sample absorbance found to be quantitatively accurate. 2D-IR and Fourier transform infrared spectroscopy of two carbonyl containing species acetone and N-methyl-acetamide dissolved in D_2O are used to experimentally confirm the validity of the ratiometric calculations. Finally, to address ambiguities over units and scaling of 2D-IR signals, a physical unit of 2D-IR spectral amplitude in $mOD/\sqrt{cm^{-1}}$ is proposed.

Reproduced from *Anal. Chem.* 2022, 94, 51, 17988–17999, under the terms of a [Creative Commons CC BY 4.0 License](https://creativecommons.org/licenses/by/4.0/). doi: 10.1021/acs.analchem.2c04287

Author: P.M. Donaldson

Contact author: P.M. Donaldson
(paul.donaldson@stfc.ac.uk)



Surface enhanced Raman scattering with a Kerr-gate for fluorescence suppression

The combination of surface-enhanced and Kerr-gated Raman spectroscopy for the enhancement of Raman signal and suppression of fluorescence is reported. The technique enables the study of analytes that show weak Raman signal in highly fluorescent media under (pre)resonant conditions. This approach was exemplified by the well-defined spectra of Nile red (NR) and Nile blue (NB). Raman spectra of the fluorescent dyes were only obtained when SERS active substrates were used in combination with the Kerr-gate. To achieve enhancement of the weaker Raman scattering, Au films with different roughness or Au-core shell-isolated nanoparticles (SHINs) were used. Crucially, the use of SHINs enabled measurement of the Raman bands of fluorescent dyes upon non-SERS active, optically flat Au, Cu, and Al substrates.

Reproduced from *J. Phys. Chem. Lett.* 2024, 15, 608-615, published by the American Chemical Society, under the terms of a [Creative Commons CC BY 4.0 License](https://creativecommons.org/licenses/by/4.0/). doi:10.1021/acs.jplett.3c02926

Authors: G. Cabello, I.V. Sazanovich, A.R. Neale, L.J. Hardwick

Contact author: L.J. Hardwick (hardwick@liverpool.ac.uk)

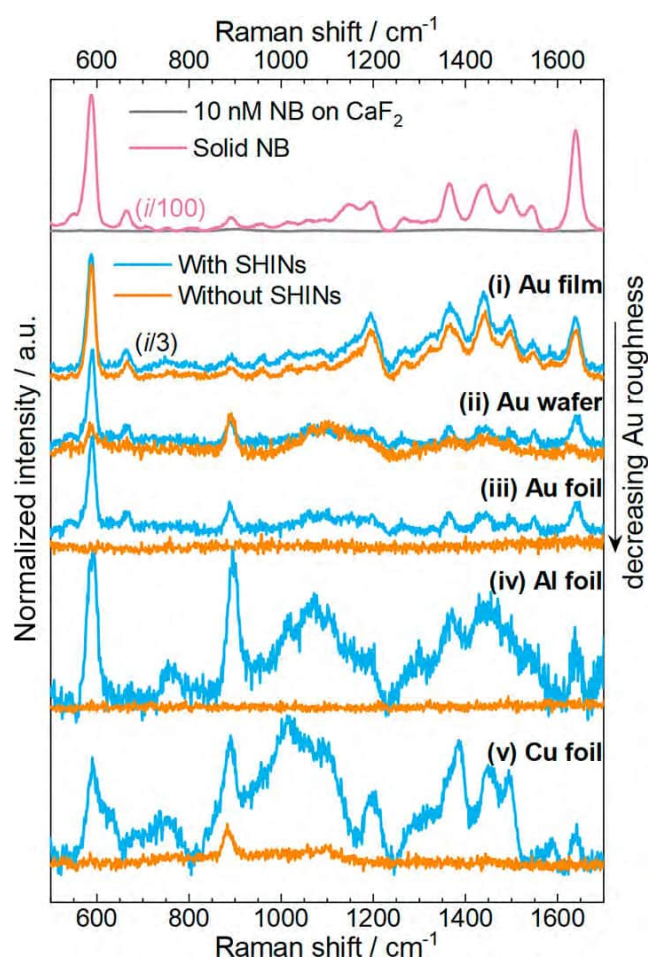


Figure 1: Kerr-gated Raman spectra for solid NB (pink), a 10 nM solution of NB in ethanol on glass (grey), and 10 nM solutions of NB in ethanol at different substrates without SHINs (orange) and with SHINs (blue): Au film, Au wafer, Au foil, Al foil, Cu foil. The intensity of spectra from Au film has been reduced three-fold. All spectra collected under 633 nm ps pulsed laser excitation.

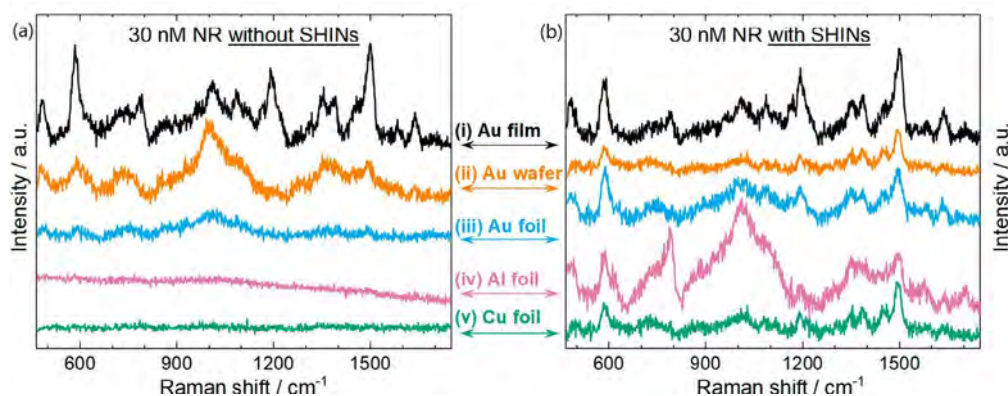


Figure 2: Kerr-gated Raman spectra, without (a) and with (b) a layer of SHINs, of a solution containing 30 nM NR in acetone on Au film (i); Au wafer (ii); Au foil (iii); Al film (iv); and Cu film (v). All spectra were collected under 633 nm ps pulsed laser excitation.

Optical Screening and Classification of Drug Binding to Proteins in Human Blood Serum

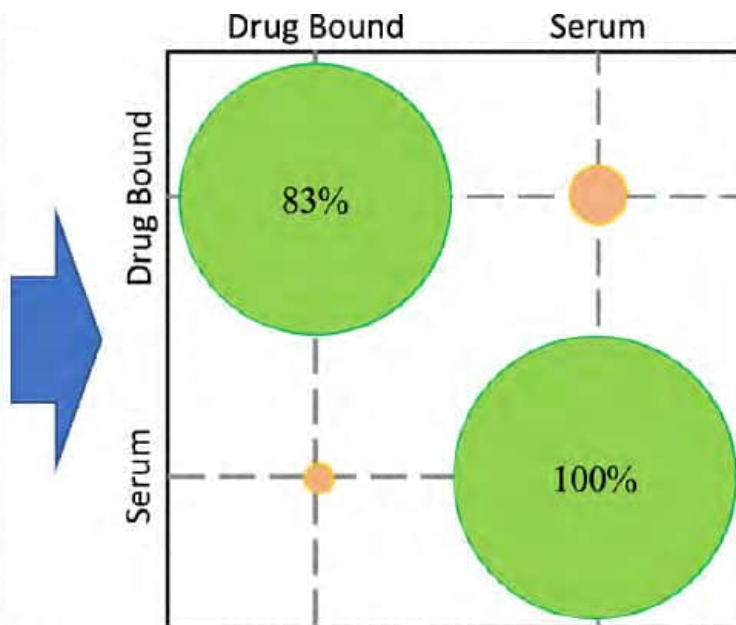
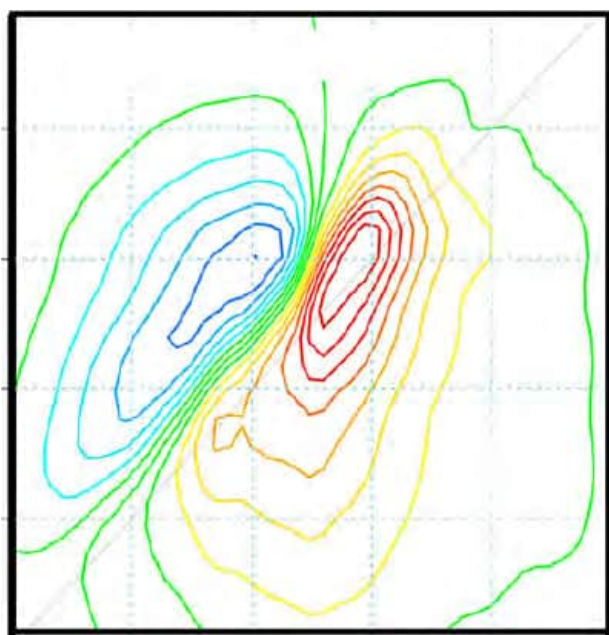
Protein–drug interactions in the human bloodstream are important factors in applications ranging from drug design, where protein binding influences efficacy and dose delivery, to biomedical diagnostics, where rapid, quantitative measurements could guide optimized treatment regimes. Current measurement approaches use multistep assays, which probe the protein-bound drug fraction indirectly and do not provide fundamental structural or dynamic information about the in vivo protein–drug interaction. We demonstrate that ultrafast 2D-IR spectroscopy can overcome these issues by providing a direct, label-free optical measurement of protein–drug binding in blood serum samples. Four commonly prescribed drugs, known to bind to human serum albumin (HSA), were added to pooled human serum at physiologically relevant concentrations. In each case, spectral changes to the amide I band of the serum sample were observed, consistent with binding to HSA, but were distinct for each of the four drugs. A machine-learning-based classification of the serum samples achieved a total cross-validation prediction accuracy of 92% when differentiating serum-only samples from those with a drug present.

Identification on a per-drug basis achieved correct drug identification in 75% of cases. These unique spectroscopic signatures of the drug–protein interaction thus enable the detection and differentiation of drug containing samples and give structural insight into the binding process as well as quantitative information on protein–drug binding. Using currently available instrumentation, the 2D-IR data acquisition required just 1 min and 10 μL of serum per sample, and so these results pave the way to fast, specific, and quantitative measurements of protein–drug binding in vivo with potentially invaluable applications for the development of novel therapies and personalized medicine.

Reproduced from Anal. Chem. 2023, 95, 46, 17037–17045, published by the American Chemical Society, under the terms of a [Creative Commons CC-BY 4.0 License](#). doi:10.1021/acs.analchem.3c03713

Authors: S.H. Rutherford, C.D.M. Hutchison, G.M. Greetham, A.W. Parker, A. Nordon, M.J. Baker, N.T. Hunt

Contact author: N.T. Hunt (neil.hunt@york.ac.uk)



Coumarin C-H functionalization by Mn(I) carbonyls: Mechanistic insight by ultra-fast IR spectroscopic analysis

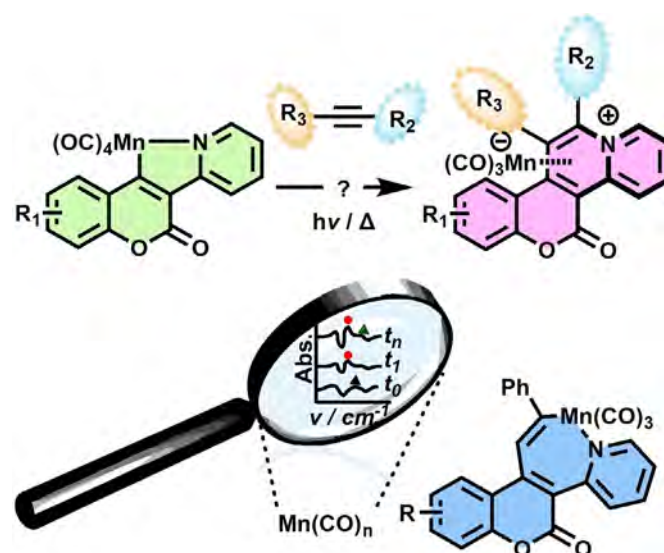
Mn(I) C-H functionalization of coumarins provides a versatile and practical method for the rapid assembly of fused polycyclic pyridinium-containing coumarins in a regioselective manner. The synthetic strategy enables application of bench-stable organomanganese reagents in both photochemical- and thermal-promoted reactions. The cyclomanganated intermediates, and global reaction system, provide an ideal testing ground for structural characterization of the active Mn(I) carbonyl-containing species, including transient species observable by ultra-fast time-resolved spectroscopic methods. The thermodynamic reductive elimination product, solely encountered from reaction between alkynes and air-stable organometallic cyclomanganated coumarins, has enabled characterization of a critical seven-membered Mn(I) intermediate, detected by time-resolved infrared spectroscopy, enabling the elucidation of the temporal profile of key steps in the reductive elimination pathway. Quantitative data are provided. Manganated polycyclic products are readily decomplexed by AgBF_4 , opening-up an efficient route to the formation of π -extended hybrid coumarin-pyridinium compounds.

Reproduced from *Chem. Eur. J.* 2023, 29, e202203038, published by Wiley-VCH GmbH, under the terms of a [Creative Commons Attribution License CC-BY 4.0](https://creativecommons.org/licenses/by/4.0/). doi:10.1002/chem.202203038

Authors: T.J. Burden, K.P.R. Fernandez, M. Kagoro, J.B. Eastwood, T.F.N. Tanner, A.C. Whitwood, I.P. Clark, M. Towrie, J-P. Krieger, J.M. Lynam, I.J.S. Fairlamb

Contact authors: J.M. Lynam (jason.lynam@york.ac.uk)

I.J.S. Fairlamb (ian.fairlamb@york.ac.uk)



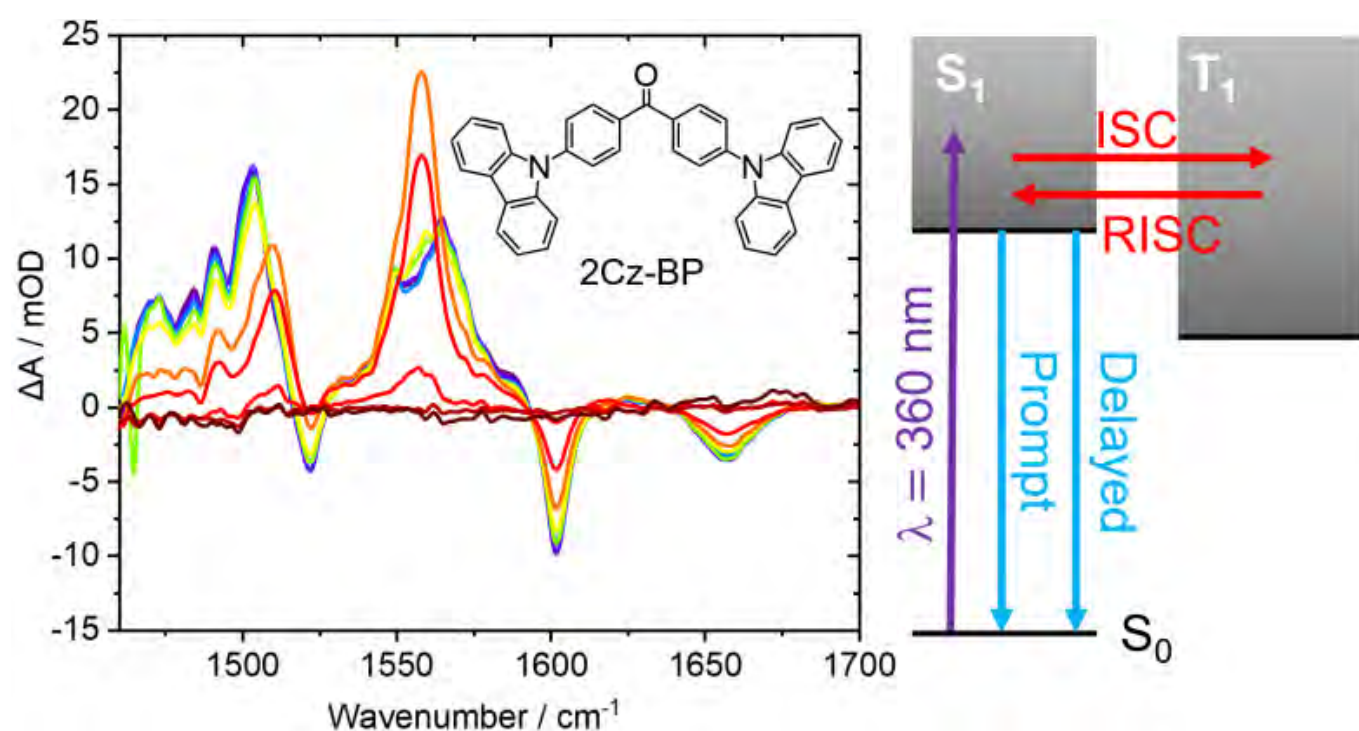
Photochemical dynamics of organic photocatalysts showing reverse intersystem crossing and thermally activated delayed fluorescence

Time-resolved infrared and fluorescence spectroscopy measurements reveal reverse intersystem crossing and delayed fluorescence emission in new designs of organic photocatalysts being tested for photoredox catalysis of atom-transfer radical polymerization. The organic photocatalysts have donor-acceptor-donor (D-A-D) structures based on a central benzophenone acceptor chromophore and pendant carbazole, phenoxazine or phenothiazine donor moieties. Comparison of the excited state relaxation timescales measured using the complementary time-resolved IR absorption and fluorescence emission techniques distinguishes organic compounds that are TADF emitters in their monomeric forms, or that only become TADF emitters upon aggregation in solution.

These contrasting behaviours account for the different efficiencies of the photocatalysts when used in photoredox catalytic cycles to initiate atom-transfer radical polymerization.

Authors: W. Whitaker, A.J. Orr-Ewing, Y. Kwon, W. Jeon, M.S. Kwon, I.V. Sazanovich

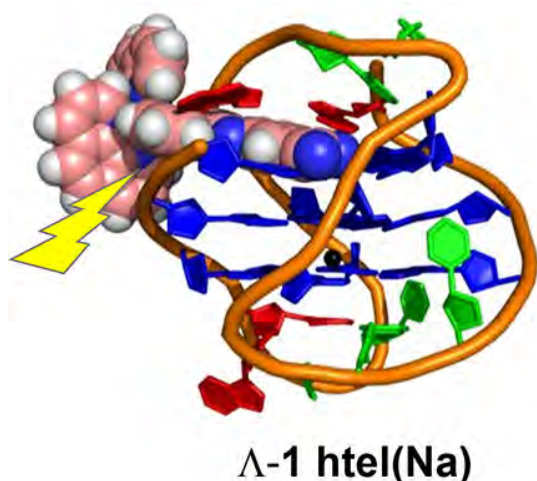
Contact author: A.J. Orr-Ewing
(a.orr-ewing@bristol.ac.uk)



Time-resolved infra-red (TRIR) spectra (left) of a solution of the carbazole-substituted benzophenone molecule 2Cz-BP show growth and decay of triplet-state population, and relaxation of S_1 population over picosecond to microsecond timescales. These observations are consistent with forward and reverse intersystem crossing (ISC and RISC), resulting in both prompt and delayed fluorescence emission. The Jablonski diagram (right) shows these competing photochemical pathways.

Good vibrations report on the DNA quadruplex binding of an excited state amplified ruthenium polypyridyl IR probe

The nitrile containing Ru(II)polypyridyl complex $[\text{Ru}(\text{phen})_2(11,12\text{-dCN-dppz})]^{2+}$ (**1**) is shown to act as a sensitive infrared probe of G-quadruplex (G4) structures. UV-visible absorption spectroscopy reveals enantiomer sensitive binding for the hybrid **htel(K)** and antiparallel **htel(Na)** G4s formed by the human telomere sequence $\text{d}[\text{AG}_3(\text{TTAG}_3)_3]$. Time-resolved infrared (TRIR) of **1** upon 400 nm excitation indicates dominant interactions with the guanine bases in the case of Λ -**1/htel(K)**, Δ -**1/htel(K)**, and Λ -**1/htel(Na)** binding, whereas Δ -**1/htel(Na)** binding is associated with interactions with thymine and adenine bases in the loop. The intense nitrile transient at 2232 cm^{-1} undergoes a linear shift to lower frequency as the solution hydrogen bonding environment decreases in DMSO/water mixtures. This shift is used as a sensitive reporter of the nitrile environment within the binding pocket. The lifetime of **1** in D_2O (ca. 100 ps) is found to increase upon DNA binding, and monitoring of the nitrile and ligand transients as well as the diagnostic DNA bleach bands shows that this increase is related to greater protection from the solvent environment.



(Left) Predicted structure of the lambda enantiomer of the $[\text{Ru}(\text{phen})_2(11,12\text{-dCN-dppz})]^{2+}$ (**1**) bound to the antiparallel G4 structure formed from the human telomere sequence $\text{d}[\text{AG}_3(\text{TTAG}_3)_3]$ in the presence of sodium ions.

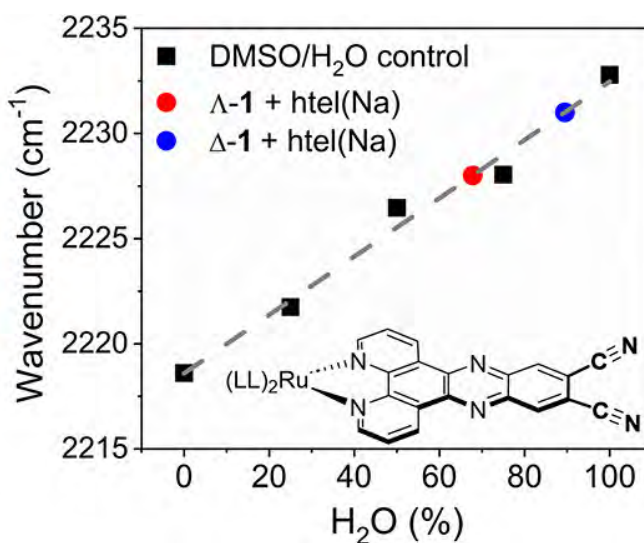
Molecular dynamics simulations together with binding energy calculations identify the most favorable binding site for each system, which are in excellent agreement with the observed TRIR solution study. This study shows the power of combining the environmental sensitivity of an infrared (IR) probe in its excited state with the TRIR DNA "site effect" to gain important information about the binding site of photoactive agents and points to the potential of such amplified IR probes as sensitive reporters of biological environments.

Reproduced from *J. Am. Chem. Soc.* 2023, 145, 39, 21344-21360, published by American Chemistry Society, under the terms of a [Creative Commons Attribution License CC-BY 4.0](https://creativecommons.org/licenses/by/4.0/). doi: 10.1021/jacs.3c06099

Authors: M. Stitch, D. Avagliano, D. Graczyk, I.P. Clark, L. González, M. Towrie, S.J. Quinn

Contact authors: L. González (leticia.gonzalez@univie.ac.uk)

S.J. Quinn (susan.quinn@ucd.ie)



(Right) Correlation of the position of nitrile transient for G4-bound Λ -1 (red circle) and Δ -1 (blue circle) to the hydrogen bonding nature of the solution environment (black squares).

G-Quadruplex Binding of an NIR Emitting Osmium Polypyridyl Probe Revealed by Solution NMR and Time-Resolved Infrared Studies

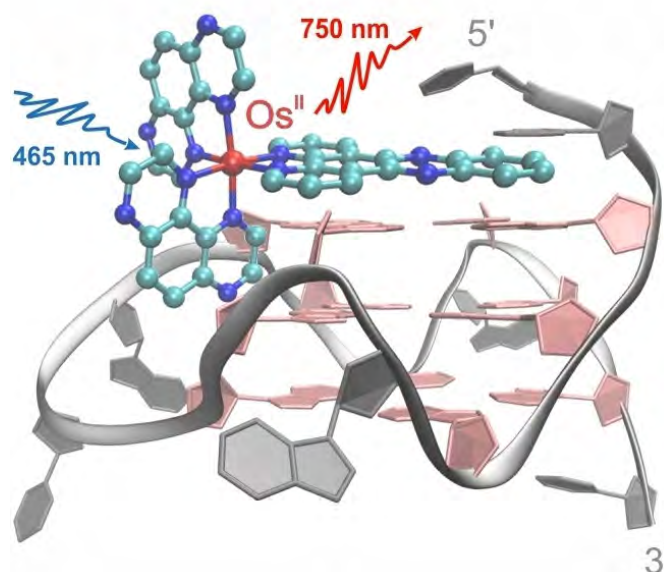
G-quadruplexes are emerging targets in cancer research and understanding how diagnostic probes bind to DNA G-quadruplexes in solution is critical to the development of new molecular tools. In this study the binding of an enantiopure NIR emitting $[\text{Os}(\text{TAP})_2(\text{dppz})]^{2+}$ complex to different G-quadruplex structures formed by human telomere (hTel) and cMYC sequences in solution is reported. The combination of NMR and time-resolved infrared spectroscopic techniques reveals the sensitivity of the emission response to subtle changes in the binding environment of the complex. Similar behaviour is also observed for the related complex $[\text{Os}(\text{TAP})_2(\text{dppp2})]^{2+}$ upon quadruplex binding.

Reproduced from *Chem. Eur. J.* 2023, 29, e202203250, published by Wiley-VCH GmbH, under the terms of the [Creative Commons Attribution License](#). doi: 10.1002/chem.202203250

Authors: K. Peterková, M. Stitch, R.Z. Boota, P.A. Scattergood, P.I.P. Elliott, M. Towrie, P. Podbevšek, J. Plavec, S.J. Quinn

Contact authors: J. Plavec
(janez.plavec@ki.si)

S.J. Quinn (susan.quinn@ucd.ie)



Structural modelling of the lambda enantiomer of the osmium polypyridyl light switch probe containing the extended dipyrido[3,2-a:2',3'-c]phenazine (dppz) ligand to the cMYC quadruplex structure (PDB ID: 2LBY). NMR studies reveal the role of π - π stacking of the dppz ligand at the 5'-quartet end, which is supported by time-resolved infrared measurements. Notably, the luminescent enhancement is found to be sensitive to the particular orientation at the 5'-quartet binding site.

A stronger acceptor decreases the rates of charge transfer: ultrafast dynamics and on/off switching of charge separation in organometallic donor–bridge–acceptor systems

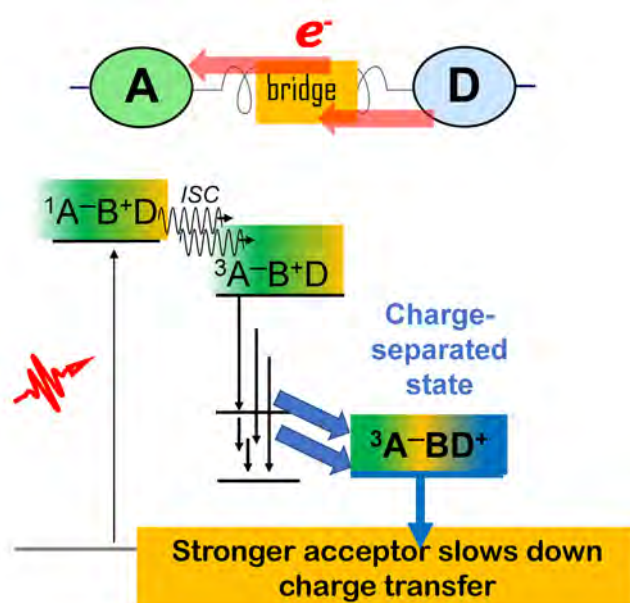
To unravel the role of driving force and structural changes in directing the photoinduced pathways in donor–bridge–acceptor (DBA) systems, we compared the ultrafast dynamics in novel DBAs which share a phenothiazine (PTZ) electron donor and a Pt(II) trans-acetylide bridge ($-\text{C}\equiv\text{C}-\text{Pt}-\text{C}\equiv\text{C}-$), but bear different acceptors conjugated into the bridge (naphthalene-diimide, NDI; or naphthalene-monoimide, NAP). The excited state dynamics were elucidated by transient absorption, time-resolved infrared (TRIR, directly following electron density changes on the bridge/acceptor), and broadband fluorescence-upconversion (FLUP, directly following sub-picosecond intersystem crossing) spectroscopies, supported by TDDFT calculations. Direct conjugation of a strong acceptor into the bridge leads to switching of the lowest excited state from the intraligand ^3IL state to the desired charge-separated ^3CSS state. We observe two surprising effects of an increased strength of the acceptor in NDI vs. NAP: a ca. 70-fold slow-down of the ^3CSS formation $-(971 \text{ ps})^{-1}$ vs. $(14 \text{ ps})^{-1}$, and a longer lifetime of the ^3CSS (5.9 vs. 1 ns); these are attributed to differences in the driving force $\Delta G_{\text{et}'}$ and to distance dependence. The 100-fold increase in the rate of intersystem crossing—to sub-500 fs—by the stronger acceptor highlights the role of delocalisation across the heavy-atom containing bridge in this process. The close proximity of several excited states allows one to control the yield of ^3CSS from $\sim 100\%$ to 0% by solvent polarity. The new DBAs offer a versatile platform for investigating the role of bridge vibrations as a tool to control excited state dynamics.

Reproduced from A.J. Auty et al. *Chem. Sci.*, 2023, **14**, 11417–11428, under a [Creative Commons Attribution 3.0 Unported License](#). doi:10.1039/d2sc06409j

Authors: A.J. Auty, P.A. Scattergood, T. Keane, T. Cheng, G. Wu, H. Carson, J. Shipp, A. Sadler, T. Roseveare, I.V. Sazanovich, A.J.H.M. Meijer, D. Chekulaev, P.I.P. Elliot, M. Towrie, J.A. Weinstein

Contact authors: J.A. Weinstein (julia.weinstein@sheffield.ac.uk)

A.J.H.M. Meijer (a.meijer@sheffield.ac.uk)



The upper part displays the schematic of a donor-bridge-acceptor system, with the acceptor being on the left, and the donor on the right, the bridge in the middle, and an arrow indicating the direction of the electron transfer. The lower part presents the schematic energy level diagram for such a system, with the photo-populated singlet $\text{A-B}^+\text{D}$ being the highest level, and the triplet state $\text{A-B}^+\text{D}$ being slightly below and getting populated promptly from the former one; the third state – the triplet and fully charge-separated A-BD^+ – is positioned significantly lower than the other two. The picture illustrates that the stronger acceptor significantly slows down the rate of the full charge-separated state formation – whilst it should have been the other way around!